Dunlop and Özdemir
Earth, Planets and Space (2018) 70:164
https://doi.org/10.1186/s40623-018-0928-z

Earth, Planets and Space

FULL PAPER Open Access

Remanence cycling of 0.6–135 μm magnetites across the Verwey transition

David J. Dunlop* and Özden Özdemir

Abstract

We report zero-field low-temperature cycling of saturation remanence (SIRM) produced at 300 or 10 K for crushed natural magnetites in nine size fractions from 0.6 to 135 μm, one set annealed to reduce stress, the other unannealed. Coercivities of isothermal remanence increase tenfold between 300 and 10 K, possibly explaining an apparent transition near 50 K. 300-K SIRM decreases continuously on cooling, losing 60–80% by $T_V = 120$ K (Verwey transition), is constant from 120 to 10 K, then recovers a small memory in warming through T_V to 300 K. A dip and recovery of remanence near T_V for larger (> 15 μm) annealed grains is probably due to memory of cubic domain structures by monoclinic magnetite below T_V, permitting partial recovery of initial remanence. In warming, 10-K SIRM is little affected until lost catastrophically near T_V. A small memory is recovered in cooling to 10 K. The contrasting behaviors of 300-K and 10-K SIRMs result from the contrasting anisotropies and domain structures of cubic and monoclinic magnetite. Memories of initial remanences after full temperature cycles are attributed to monoclinic magnetite providing a template for partially regenerating initial cubic domain structures on the second passage through T_V. Memory ratios as a function of grain size for our magnetites are too scattered to be granulometrically useful.

Keywords: Magnetite, Verwey transition, Saturation remanence, Low-temperature cycling

Introduction

Magnetite (Fe_3O_4) is cubic at room temperature with inverse spinel structure. Its first magnetocrystalline anisotropy constant K_1 is negative and the easy axes for spontaneous magnetization $\boldsymbol{M}_s$ are the four ⟨111⟩ body diagonals. Below room temperature, magnetite undergoes at least two transitions. At the isotropic point near 130 K, K_1 changes sign and the easy axes switch to ⟨001⟩. Domain structures must change as a result but there is usually little sign of this in the measured sample magnetization.

The Verwey transition (Verwey 1939; Walz 2002) near 120 K is a first-order phase transition. The cubic lattice deforms only slightly and exchange interaction is scarcely affected, as evidenced by the near-continuity of M_s across the transition (e.g., Özdemir 2000; Kosterov 2001), but the magnetocrystalline anisotropy constants of the new monoclinic lattice increase more than tenfold. $\boldsymbol{M}_s$ now lies along an easy c-axis which is one of the cubic ⟨001⟩ axes. Less reorganization of domains would seem to be required than at the isotropic point, but there are two complications. The anisotropy is no longer multiaxial, with the possibility of 90° walls and closure structures as well as 180° walls (Özdemir et al. 1995), but uniaxial. In addition, within each grain monoclinic twinning typically produces a mosaic of twin domains with different c-axes, minimizing overall crystal strain (Salje 1993).

A variety of techniques have imaged either magnetic domain walls (DWs) (Moloni et al. 1996; Carter-Stiglitz et al. 2006) or twin walls (TWs, the boundaries between twin domains) (Chikazumi et al. 1971; Otsuka and Sato 1986; Medrano et al. 1999), but not both simultaneously. In a recent breakthrough, Kasama et al. (2010, 2013) and Bryson et al. (2013) have imaged interacting DWs and TWs using transmission electron microscopy (TEM). Magnetic structure was obtained both with Fresnel imaging in Lorentz TEM and by off-axis electron holography (Harrison et al. 2002). TWs impede DW motion. When a 180° DW reaches a TW, it cannot pass into a neighboring twin domain whose easy c-axis is rotated by 90°. In

*Correspondence: dunlop@physics.utoronto.ca
Department of Physics, University of Toronto, Toronto, ON M5S 1A7, Canada

addition, the TW is a site of spontaneous lattice strain; magnetoelastic interaction must add to DW pinning (Xu and Merrill 1989).

Indirect evidence for domain reorganization and DW pinning at the Verwey transition is provided by remanence cycling and magnetic hysteresis experiments across the transition region (e.g., Hartstra 1982, 1983; Hodych 1986, 1991; Halgedahl and Jarrard 1995; Özdemir and Dunlop 1998, 1999; Muxworthy 1999; King and Williams 2000; Muxworthy and McClelland 2000; Özdemir 2000; Kosterov 2001, 2003; Özdemir et al. 2002; Smirnov and Tarduno 2002; Muxworthy et al. 2003; Yu et al. 2004; Smirnov 2006, 2009; Kosterov and Fabian 2008). The present paper adds to this body of measurements, filling a data gap between the submicron and mm-size magnetites studied by Özdemir et al. (2002) and complementing the hysteresis study of Dunlop et al. (2018) on the same set of samples used here.

The first purpose of our study was to use well-sized magnetites from a common source (see "Sample characterization and experimental methods" section) to test how low-temperature remanence cycling varies with magnetite grain size. A second purpose was to investigate the effect of internal stress. The ferroelastic properties of monoclinic magnetite (Salje 1993) imply that internal stress should be particularly influential at and below the Verwey transition.

Sample characterization and experimental methods

Our samples used natural magnetite single crystals from the Princess Quarry in Bancroft, ON, Canada, a source of museum-quality mineral specimens. Purity of these crystals was tested by X-ray diffraction and the Curie temperature T_C. Only the X-ray lines of stoichiometric magnetite were observed; there were no rhombohedral or secondary spinel reflections of hematite and maghemite. T_C was 580 °C, the Curie point of stoichiometric magnetite. Identical Curie points were obtained for the crushed sized fractions described below (Dunlop 2014).

Experiments were performed on carefully sized fractions of magnetite. The crystals were first crushed by mortar and pestle. Two coarse size fractions were obtained by sieving, and seven fine fractions were separated from the post-sieve residue using a Bahco centrifugal dust analyzer. The mean sizes of the fine fractions span a broad range, from 20.0 ± 4.6 μm to 0.615 ± 0.30 μm (arithmetic means), with relatively small overlap between fractions (Table 1). For convenience, dust fraction samples are referred to in the rest of the paper by their mean grain sizes rounded off to the nearest whole number; for example, the 6 μm sample refers to the 5.85 μm fine fraction. The coarse fractions are also named according to mean size, 135 μm for the 125–150 μm and 110 μm for the 100–125 μm sieve fractions. Scanning electron micrographs and size distributions appear in Dunlop et al. (2018, Figs. 1, 2). Size distributions are symmetrical about the mean and approximately Gaussian for the 20 μm, 14 μm and 9 μm samples, somewhat skewed to small sizes for the 6 μm sample, and approximately lognormal for the 3 μm, 1 μm and 0.6 μm samples.

Table 1 Grain size and shape determinations for the magnetite samples

Setting[a]	Nominal grain size (μm)	Grain width (μm)	Dispersion (μm)	Axial ratio[b]
Sieved	135	125–150[c]		
Sieved	110	100–125[c]		
4	20	20.0	±4.6	1.52
8	14	14.1	±3.7	1.39
12	9	8.95	±2.7	1.45
14	6	5.85	±2.25	1.46
16	3	2.95	±1.15	1.49
17	1	0.955	±0.50	1.43
18	0.6	0.615	±0.30	1.49

[a] Standard settings of plate spacings in Bahco dust analyzer

[b] Grain length/width ratio

[c] Range of mesh sizes

Despite some overlap between size distributions, our samples are probably as narrowly sized as is possible using a dust analyzer. This is an important point because a major objective of this study was to test the variation of magnetic properties with grain size. Maximizing the number of samples obtainable from the available material requires some trade-off with size overlap between samples.

Another purpose of the study was to test the effect of internal stress on magnetic properties. To this end, two sets of samples were prepared. Samples in the first set were unannealed, while samples in the second set were annealed in vacuum for 7 h at 700 °C. Samples were measured as undispersed powders. Previous work (Yu et al. 2004, Fig. 7) has shown very little difference in the hysteresis properties of bulk powders and 0.5% dispersions of synthetic magnetites ranging from 0.24 μm to 16.9 μm in size, presumably because interacting particle clumps are very difficult to break up.

Temperature cycling of saturation isothermal remanent magnetization (IRM), imparted at either 300 K or 10 K, was performed using Quantum Design Magnetic Properties Measurement Systems (MPMS) with SQUID (superconducting quantum interference device) detectors at the Institute for Rock Magnetism, University of Minnesota and at the Department of Earth Sciences,

Kyoto University. The dependence of IRM intensity on magnetic field strength was also measured using the MPMS.

Results

Isothermal remanence as a function of field strength

The magnetocrystalline anisotropy and magnetostriction constants of monoclinic magnetite below the Verwey transition ($T_V \approx 120$ K) are more than an order of magnitude higher than those of cubic magnetite above T_V (Bickford et al. 1957; Syono 1965; Abe et al. 1976; Tsuya et al. 1977; Kakol et al. 1991, 1994). The result is that isothermal remanence requires much higher fields to reach saturation below T_V than above (Fig. 1). The spectrum of coercivities measured at 10 K extends at least as high as 5 T, while at 300 K a field of 0.2 T will saturate the IRM. In what follows, saturation IRM was produced by a 2 T field at 300 K and by a 5 T field at 10 K.

Temperature cycling of 300 K saturation remanence

A set of results for the 1 μm, 6 μm, 9 μm and 14 μm annealed magnetites appears in Fig. 2. Data were measured during cooling at 10 K intervals from 300 to 130 K and from 80 to 10 K and at 5 K intervals from 120 to 90 K. During warming, the same measurement intervals were used. There is a continuous loss of 70–80% of the starting remanence in cooling from 300 K to ≈115 K, accelerating below 150 K as the Verwey transition approaches. There is no indication in the data of the isotropic point around 130 K where the cubic easy axes switch from ⟨111⟩ to ⟨001⟩. The point of steepest descent in the cooling curves is taken to indicate the Verwey transition temperature T_V (Table 2).

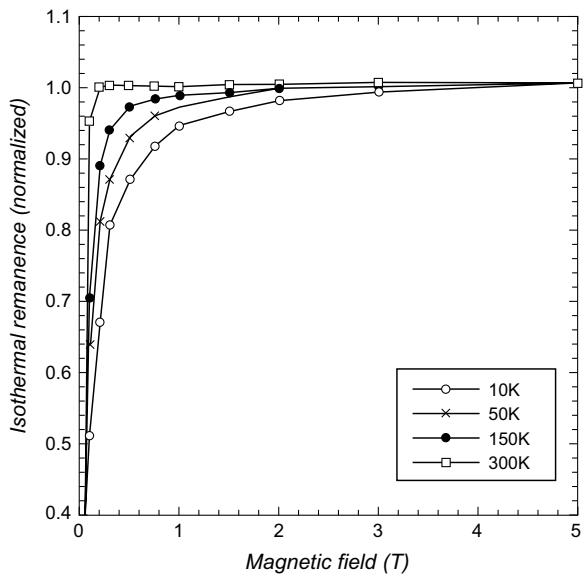

Fig. 1 Acquisition of isothermal remanent magnetization (IRM) as a function of applied magnetic field measured at various temperatures for the 0.6 μm annealed magnetite sample

A small loss of remanence continues below T_V but the cooling curves level out below 80 K. In the warming half-cycle from 10 K, the remanence is almost unchanging until 100–110 K and then recovers a small amount—the so-called memory—in passing from the monoclinic to the cubic phase at T_V. For the 14 μm sample, there is a small dip and recovery of remanence around 115 K, close to $T_V = 118$ K measured in cooling. This dip is not seen for smaller grain sizes.

Figure 3 zooms in on the Verwey transition region for the 14 μm and larger annealed magnetites. Now it becomes clear that the warming remanence reaches a peak between 100 and 105 K before beginning to decrease between 105 and 120 K. The minimum near T_V becomes more marked at larger grain sizes. A matching, although smaller, dip to a minimum can be seen in the cooling curves as well for the 110 μm and 135 μm samples.

Figure 4 compares data for the unannealed and annealed 135 μm magnetites. A higher level of internal stress reduces the peak and dip in the warming curve of the unannealed 135 μm magnetite compared to its annealed counterpart, while the dip and peak in the cooling curve are completely suppressed in the unannealed sample. The structural changes occurring during the monoclinic → cubic transformation and, even more so, the changes in the cubic → monoclinic transformation during cooling evidently are sensitive to internal stress.

Turning to even larger grain sizes, Fig. 5 demonstrates a rather striking similarity in the behavior of the 14 μm annealed sample and a 1.5 mm single crystal of magnetite. Both exhibit peaks in remanence at 105–110 K during warming followed by a plunge to a minimum at $T_V = 115$–120 K. The 1.5 mm crystal exhibits identical behavior in its cooling curve, whereas the cooling curve of the 14 μm sample is equivocal.

Temperature cycling of 10 K saturation remanence

Figure 6 illustrates warming curves of saturation remanence produced at 10 K in unannealed samples. Each saturation IRM was produced after zero-field cooling (ZFC) of a demagnetized sample from 300 K. Cooling half-cycles were not measured, but the ultimate remanences at 10 K (the individual dots at the left) are very similar to the 300 K values. The Verwey transition in the warming curves is marked by a simple featureless decrease in remanence, without any peak, dip or recovery like those seen in the warming curves of 300-K saturation

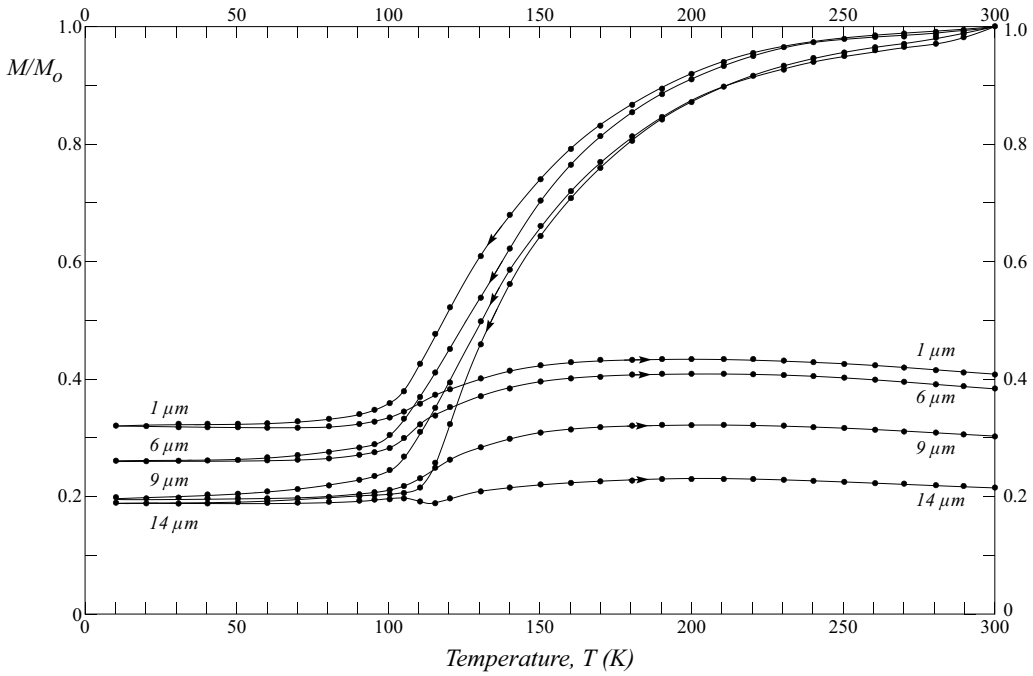

Fig. 2 Temperature dependence of saturation IRM produced by a field of 2 T at 300 K, cooled in zero field to 10 K and warmed in zero field back to 300 K for four magnetite samples. Only the 14 μm magnetite shows a dip and recovery of remanence at T_V (≈115 K)

remanence. T_V is again taken to be the point of steepest descent (Table 2). Above T_V, the curves are flat and featureless, whereas the corresponding warming curves of Fig. 2 traced a gentle arch between 120 and 300 K. Remanence imparted to the monoclinic phase seems to lack the memory capacity that the cubic phase remanence retains even after it has been transformed to the monoclinic phase and back.

Table 2 Transition temperatures T_V estimated from points of steepest descent in first crossings of the Verwey transition, while cooling 300-K SIRMs and warming 10-K SIRMs

Grain size (μm)	Annealing	T_V (K), cooling	T_V (K), warming
135	Annealed	122	112
110	Annealed	120	
20	Annealed	116	114
14	Annealed	118	110
9	Annealed	116	110
6	Annealed	108[a]	110
3	Annealed	107[a]	
1	Annealed	112	112
135	Unannealed	122	115
20	Unannealed		118
14	Unannealed		120
9	Unannealed		120
3	Unannealed		120
1	Unannealed		120

[a] Uncertain because of noisy data

Remanence warming curves for the annealed samples (Fig. 7) have a number of features lacking in the unannealed sample results. First, for the three smallest grain sizes in particular, there is a marked remanence decrease during warming from 10 K to 50 K, after which the curves level out in approaching the Verwey transition region. Second, the decrease in remanence across the Verwey transition is sharper than for the unannealed samples. Third, the remanence above T_V decreases noticeably with warming for the smaller grain sizes but after recooling to 10 K, the remanence recovers or increases compared to values at T_V for all grain sizes.

The zoom-in views of Fig. 8 illustrate the sharpness of remanence changes across the Verwey transition region in annealed samples. 70–80% of the total change occurs in the 10 K temperature interval from 105 to 115 K. In unannealed samples, the remanence drop is broader and more gradual and the upper termination of the change is close to 130 K. In annealed samples, the elbow marking the termination of the remanence drop is precisely at $T_V = 115–120$ K. In an earlier study (Dunlop et al. 2018, Fig. 7), changes in hysteresis parameters were sharper for annealed than for unannealed dust fraction separates (although not for sieved fractions).

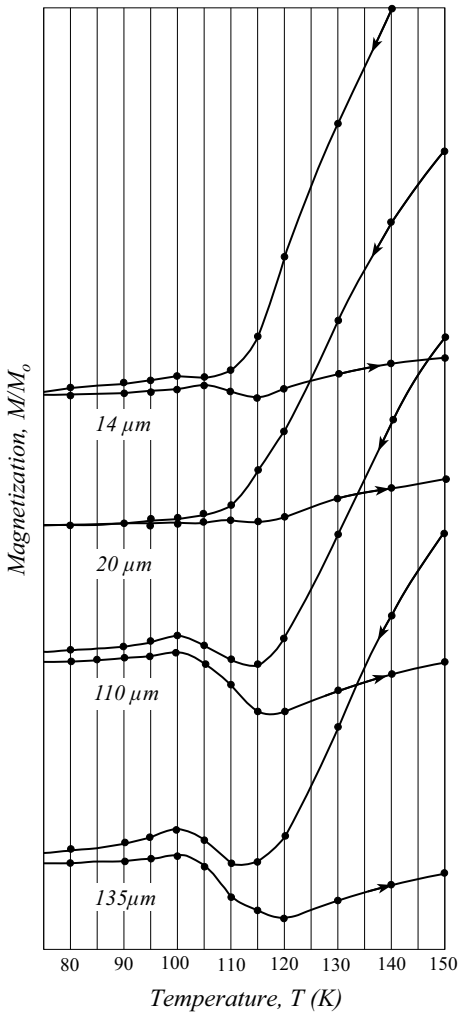

Fig. 3 Zero-field cooling and warming curves of 300-K saturation IRM over the 75–150 K interval, centered on T_V, for four larger grain size magnetites. All show a dip and recovery of remanence at T_V to varying degrees in the warming curves; the 110 and 135 μm samples show it also in their cooling curves

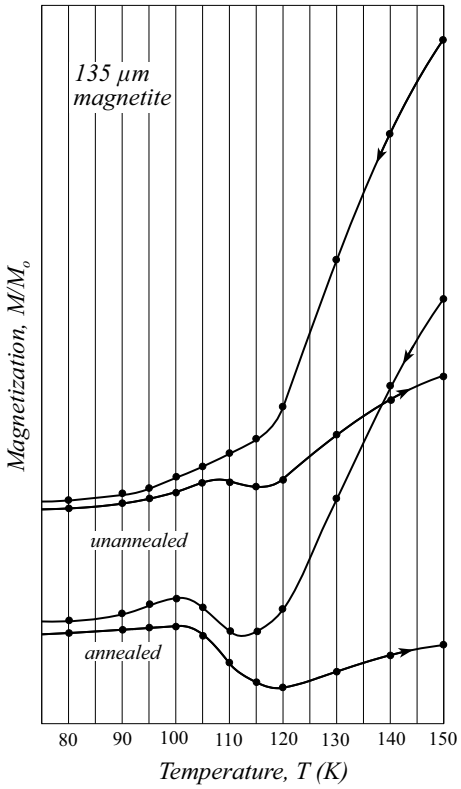

Fig. 4 Zero-field cooling and warming curves of 300-K saturation IRM for the unannealed and annealed 135 μm magnetites. In the unannealed samples, the remanence dip and recovery at T_V is much reduced in the warming curve and absent from the cooling curve

Low-temperature memory ratios

In the early days of paleomagnetism, low-temperature demagnetization (LTD) by zero-field cycling through T_V was widely investigated as a nondestructive means of selectively cleaning low-stability remanence carried by magnetite (e.g., Ozima et al. 1964; Creer and Like 1967; Kobayashi and Fuller 1968; Merrill 1970). The idea of continuous tracking to delineate the temperature spectrum of demagnetization came much later (e.g., Dunlop 2003). In the 1990s, memory ratios of remanence intensity before and after LTD were linked to magnetite grain sizes in two careful studies by Heider et al. (1992) and Halgedahl and Jarrard (1995) and proposed as a potential granulometric tool. Although this suggestion was not put to much practical use in the years that followed, it is interesting to test the idea using the data from the present paper.

King and Williams (2000) point out that the original notion of a memory ratio involved the recovery, or memory, of remanence that had been lost in crossing the Verwey transition. For convenience, we will use a looser definition, a simple ratio of the remanence remaining at the end of a temperature cycle or half-cycle to the starting remanence. In Fig. 9a, the half-cycle and full-cycle ratios $R_1 = M_{10}/M_{300}$ and $R_2 = M'_{300}/M_{300}$ for the annealed magnetites are seen to decrease roughly as log d, where d is mean grain size but the dispersion about the mean lines is too great for any practical application. Furthermore, R_1 and R_2 for the 110 and 135 μm magnetites do not fit the lines defined by the 1–20 μm data. In Fig. 9b, the half-cycle memory ratios for saturation remanences produced at 10 K are plotted for both annealed and unannealed magnetites. These ratios more or less follow single lines, except for the 0.6 μm data.

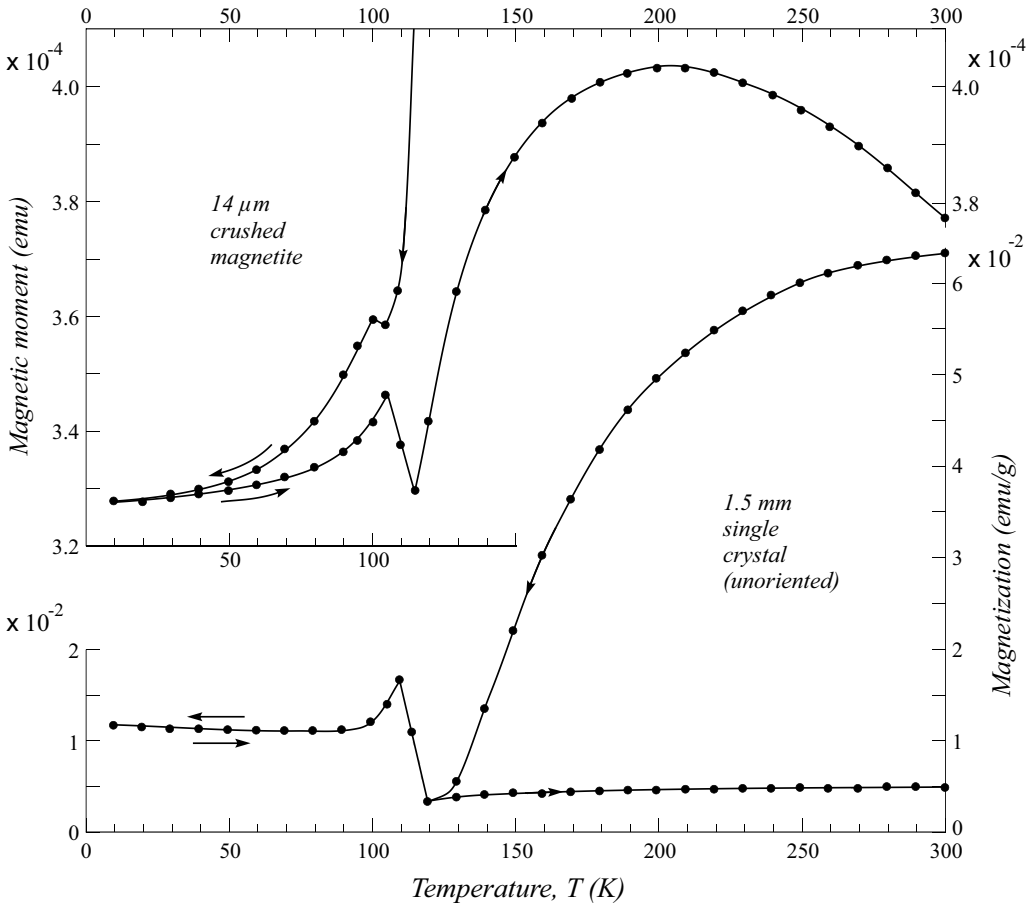

Fig. 5 Zero-field cooling and warming curves of 300-K saturation IRM for the 14 μm crushed and annealed magnetite sample and for a 1.5 mm natural magnetite crystal. Similar dips and recoveries of remanence are seen at T_V in these very different grain sizes of magnetite

Discussion

Is there a phase transition at 50 K?

The IRM acquisition curves of Fig. 1 show that monoclinic magnetite at and below 50 K has a spectrum of coercivities 10–20 times harder than that of room temperature cubic magnetite. This observation fits with measurements of the temperature dependence of coercive force H_c (Dunlop et al. 2018, Figs. 5, 6) in which H_c increases by a factor of ≈ 5 after cooling the sample through the Verwey transition, and by a further smaller amount below 50 K. Is there a true phase transition at 50 K or is this a point at which anisotropy and/or magnetostriction constants begin to increase? There is no indication of a sudden change in anisotropy or magnetostriction around 50 K in the data of Abe et al. (1976) or Kakol et al. (1994), but it is evident in Fig. 1 that individual coercivities are almost twice as large at 10 K as at 50 K.

Magnetic susceptibility undergoes changes below 40–50 K which are not generally manifested in remanence data (Muxworthy 1999; Kosterov 2003; Özdemir et al. 2009). Magnetic viscosity is also affected (Muxworthy and Williams 2006). These effects are usually attributed to diffusion after-effect and disaccommodation of susceptibility rather than to any phase transition (Walz 2002; Walz and Kronmüller 1991).

In the warming curves of 10-K saturation IRM for the annealed magnetites (Fig. 7), the three finest grained samples (1, 6 and 9 μm) have a clear inflection at 50 K between a segment of rapid remanence loss from 10 to 50 K and a more slowly descending portion from 50 to 80 K. However, this inflection is doubtful for 14 μm and larger magnetites and is completely absent from the corresponding unannealed magnetite warming curves. It is also absent from the cooling or warming curves of 300 K saturation remanence for the 1, 6 and 9 μm samples (Fig. 2). Thus, 50 K likely does not mark a structural change in magnetite, which should manifest itself in originally cubic magnetites transformed to monoclinic by cooling to 10 K, but the end of a rapid decline

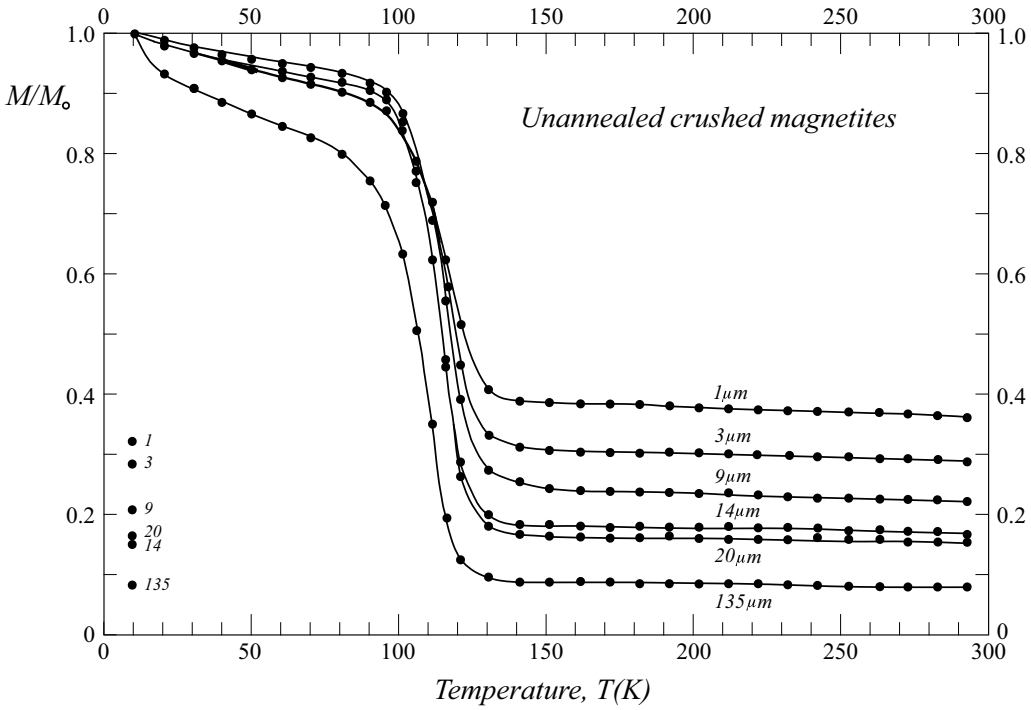

Fig. 6 Zero-field warming curves of saturation IRM produced by a field of 5 T at 10 K for six unannealed crushed magnetites. Compared to Fig. 2, the curves are rather featureless, particularly above T_V. Cooling curves were not measured but the remanences after cooling back to 10 K are shown as individual points at the left. In most cases these are virtually identical to the values measured at 300 K, indicating zero recovery of remanence in the second crossing of T_V

in coercivity that unpins about 20% of the remanence of monoclinic grains magnetized at 10 K. Why coarser annealed grains and all the unannealed magnetites are unaffected is unclear.

Cycling room temperature remanence through the Verwey transition

The Verwey transition is well expressed in all remanence cycling experiments (although the isotropic point is invisible, as in most previous studies). But its expression depends on grain size, annealing, and the nature of the phase given the initial remanence—monoclinic or cubic.

Remanence given to cubic magnetite at 300 K is already reduced by 70–80% at $T_V = 115–120$ K (Fig. 2) because of the steady decline in anisotropy and magnetostriction over this temperature range (Hodych 1986; Özdemir 2000). In the next ≈20 K of cooling, the remanence continues to change on a smaller scale, as do the magnetic hysteresis parameters of these same samples (Dunlop et al. 2018, Fig. 7). The Verwey transition has a sharp onset, as monoclinic phase nuclei appear and their boundaries propagate rapidly, but the disappearance of the cubic phase does not mean the end of all change. Kosterov and Fabian (2008) found that below T_V, more frequent and larger jumps occurred in M vs. T curves of individual grains compared to above T_V. The main mechanism of change is likely the continuing evolution of the mosaic of monoclinic twins and their TWs (Kasama et al. 2010, 2013). DWs trapped within twin domains and pinned at twin boundaries can move limited distances as the twin domains shift their positions and sizes. Arrays of mobile 180° DWs observed by Kasama et al. (2013) in occasional large untwinned monoclinic regions may also play a role.

More intriguing and not explained in any obvious way are the remanence minima centered on T_V in 14 μm and larger annealed magnetites (Fig. 3). These become quite accentuated in the 110 and 135 μm annealed samples and in a 1.5 mm magnetite crystal (Fig. 5), where they appear in both cooling and warming half-cycles, evidence that the underlying magnetoelastic phenomena causing them are reversible. What could be causing the remanence to spontaneously increase in cooling through the 15–20 K interval below T_V and to decrease even more markedly in the warming half-cycle?

Although not remarked upon in any detail in most cases, similar magnetization dips and recoveries have been observed previously in cycling 300-K remanences (Hartstra 1982, 1983; Halgedahl and Jarrard 1995; Özdemir and Dunlop 1999; Muxworthy and McClelland

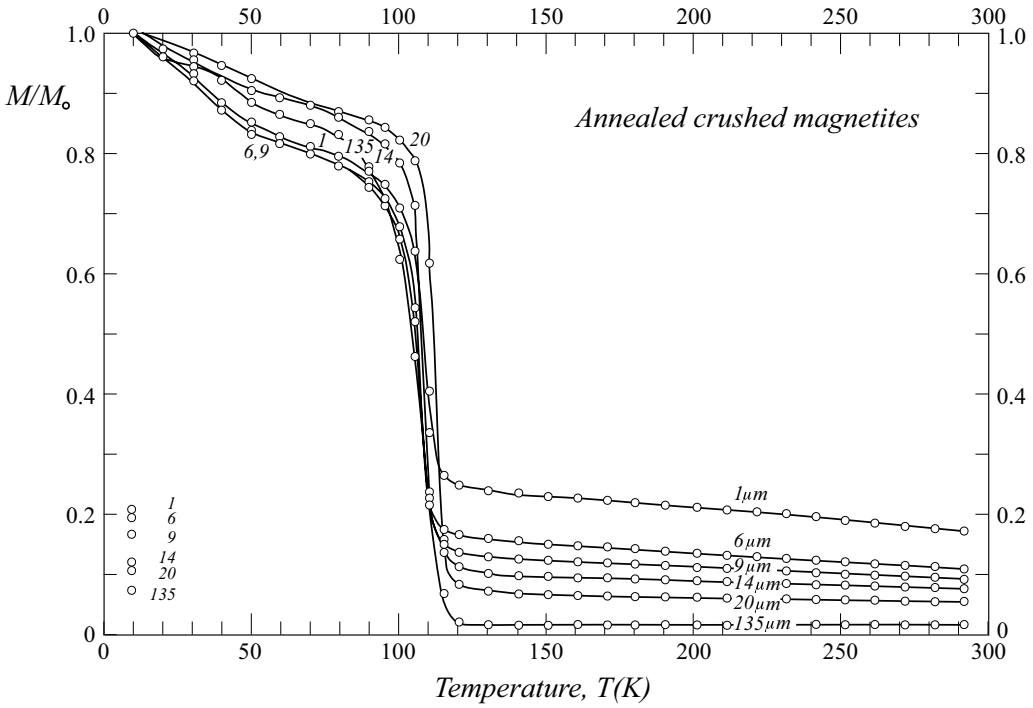

Fig. 7 Zero-field warming curves of saturation IRM produced by a field of 5 T at 10 K for six annealed crushed magnetites. Compared to the results for unannealed samples (Fig. 6), the remanence demagnetizes more between 10 and 100 K, with an inflection point at 50 K; the remanence loss at T_V is larger and more sudden; and the remanence decreases further above T_V for most grain sizes. There is substantial recovery of remanence after recooling to 10 K for the larger grain sizes

2000; King and Williams 2000; Özdemir et al. 2002; Kosterov 2003). They are usually associated with the larger grain sizes. In Hartstra's studies of sized crushed magnetites, dip and recovery was well developed in 150–250 μm, 100–150 μm and 25–30 μm grains, just detectable in 10–15 μm grains but absent from the data for < 5 μm grains. Kosterov (2003, Fig. 2), using two of Hartstra's HM4 magnetites, found a similar result. These observations accord well with ours.

Halgedahl and Jarrard (1995) detected a dip and recovery below 120 K only in a mm-size crystal. There was no remanence dip in any of their glass–ceramic magnetites, spanning sizes of 0.2, 1.5, 7 and 100 μm. Glass–ceramic magnetites (Worm and Markert 1987) are well known to have high internal stresses because of their confinement in a glass matrix, and indeed we observe in the present study that internal stress in unannealed samples reduces the dip-and-recovery effect, particularly in the cooling curve (Fig. 4).

On the other hand, in studying low-stress hydrothermal magnetites Muxworthy and McClelland (2000), reported well-developed minima, mainly in warming curves, for 3 μm, 7.5 μm and 39 μm grains but a very muted effect for 108 μm grains. A natural 190 μm magnetite, however, had remanence minima in both cooling and heating. Özdemir et al. (2002), studying even finer hydrothermal magnetites with mean sizes of 37, 100 and 220 nm, found minima at T_V in cooling curves, but more prominent were large irreversible drops in remanence between 100 and 115 K on rewarming the samples, with little or no recovery above T_V.

The bulk of the evidence favors magnetites with low internal stress and grain sizes > 15 μm as the typical natural candidates for remanence rebound just below T_V. Thus, stress, which favors stronger DW pinning, inhibits the phenomenon, while grain sizes above the nominal pseudo-single-domain (PSD)-multidomain (MD) boundary promote it, presumably for the same reason: larger numbers of more mobile DWs. Smirnov (2006) and Roberts et al. (2017) argue that the PSD state is a physically distinct magnetic state and not a mix of single-domain (SD) and MD states as modeled by Dunlop (2002). In either case, most of the grain sizes typically displaying dip and recovery are large enough to contain at least a few well-developed DWs.

The rebound of remanence in cooling below T_V is reminiscent of the memory phenomenon, in which a certain fraction of the initial 300-K remanence is recovered in the second passage through T_V. One difference is that memory persists in warming to room temperature,

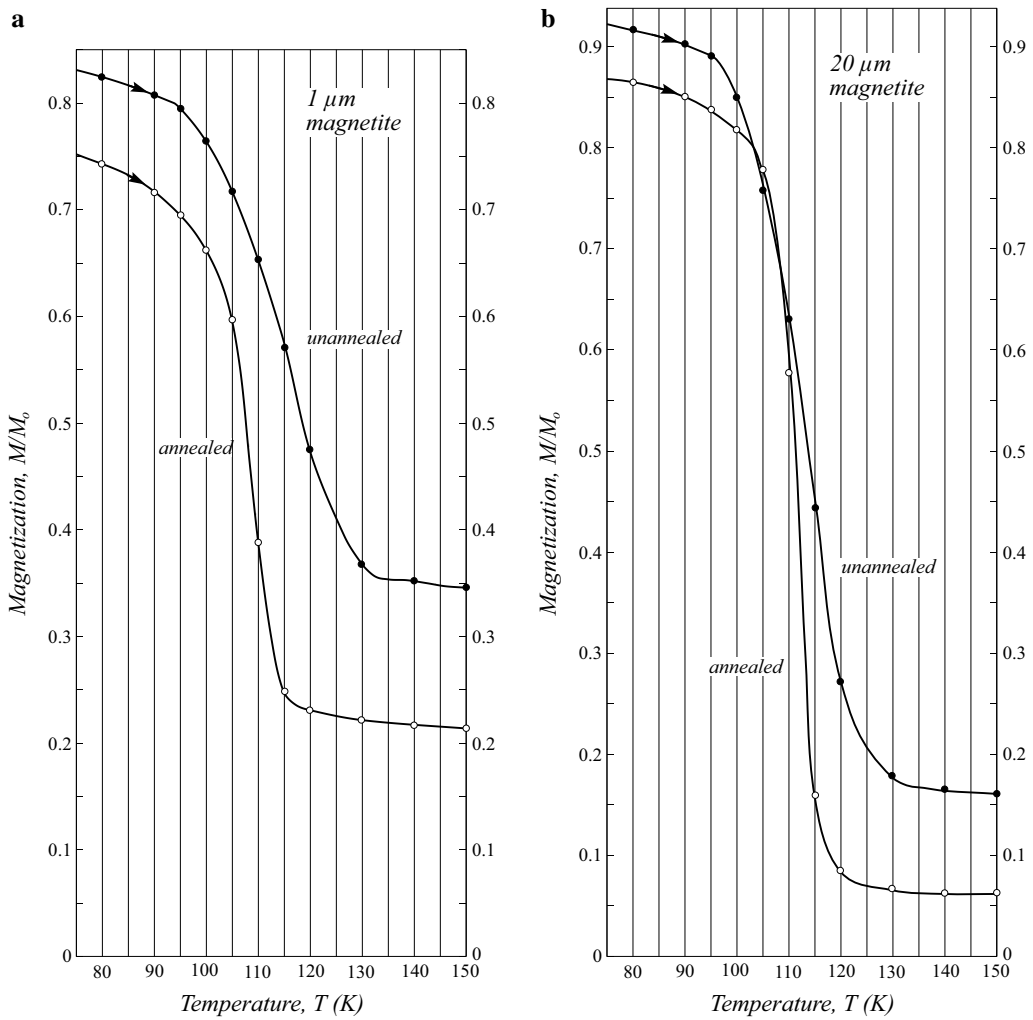

Fig. 8 An illustration of the sharpness of remanence loss in warming 10-K saturation IRM across the Verwey transition for the annealed compared to the unannealed magnetites. 60–80% of the remanence is lost between 105 and 115 K for the annealed samples. Grain sizes: **a** 1 μm; **b** 20 μm

whereas the rebound gain of remanence is largely transitory and disappears with further cooling. Muxworthy and McClelland's (2000) explanation for the rebound, which they call a positive anomaly, is the removal of screening soft DWs, revealing a hard domain structure carrying a net moment in the direction of the initial remanence. While this might be reasonable for the PSD-size hydrothermal grains that display the anomaly in their sample set, it is doubtful for the larger MD-size natural magnetites that more typically show rebound in other studies, including ours. Also if screening walls in the cubic phase are removed at T_V, why should the positive anomaly persist as the monoclinic twin and domain structures evolve during a further 15–20 K of cooling?

Cycling low-temperature remanence through the Verwey transition

Cubic magnetite magnetized at 300 K has already irreversibly lost 70–80% of its saturation remanence when it reaches T_V. Little remanence is lost in crossing T_V; indeed more typically remanence is gained. In contrast, monoclinic magnetite magnetized at 10 K loses only 10–25% of its saturation remanence in warming to 100 K, but a further 50–80% disappears between 100 and 120 K (Figs. 6, 7). The plunge is particularly precipitous for annealed samples with more easily unpinned DWs where up to 70% of the remanence disappears in the interval 105–115 K (Fig. 8). There is no sign of any dip and recovery at or near T_V.

Domain states change with temperature in both cubic and monoclinic magnetite as a result of changes in anisotropy. For example, our 6 μm annealed magnetite

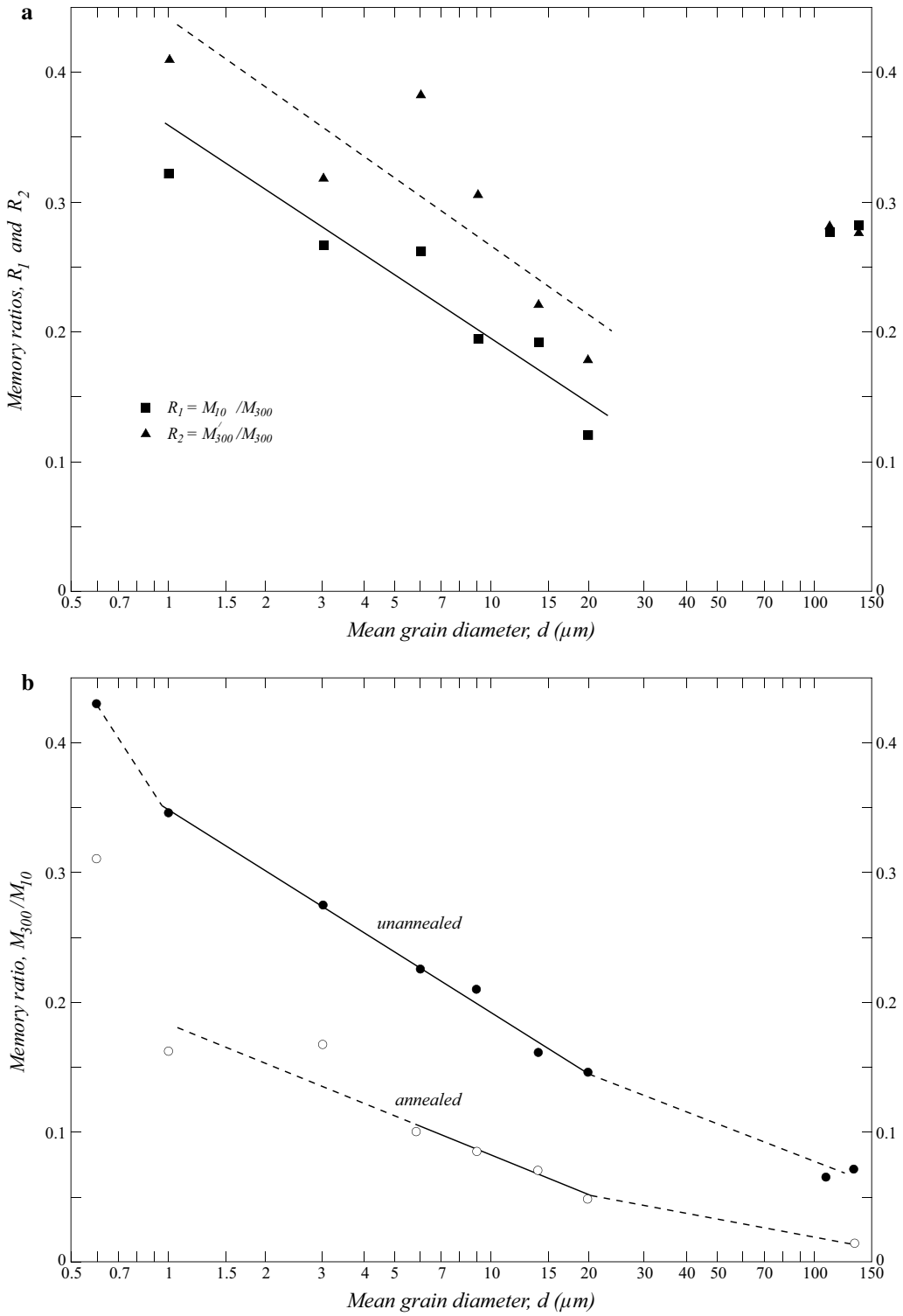

Fig. 9 Memory or remanence recovery ratios as a function of grain size for **a** 300-K saturation IRM cycled to 10 K and back to 300 K, and **b** 10-K saturation IRM cycled to 300 K and back to 10 K. In **a** the full-cycle ratio $R_2 = M'_{300}/M_{300}$ is more easily measured and more practical but shows more scatter than the half-cycle ratio $R_1 = M_{10}/M_{300}$. Neither data trend incorporates the results for the 110 and 135 μm magnetites, whose room temperature memories are anomalously high. In **b**, the half-cycle memory ratios M_{300}/M_{10} come closer to lying on a single trend. Full-cycle ratios (not plotted) are similar to the half-cycle ratios

sample has PSD hysteresis properties when magnetized in the cubic phase at room temperature, but its hysteresis properties are MD as it approaches T_V (Dunlop et al. 2018, Fig. 9). In the monoclinic phase, it rapidly hardens and when it reaches 10 K it has the hysteresis properties of a small PSD grain, approaching SD size. Thus, all our samples when magnetized as monoclinic magnetite at 10 K have more PSD- or SD-like behavior—fewer and/or less mobile DWs—than they have when magnetized as cubic magnetite at 300 K. This helps explain why so much more of the cubic phase remanence is demagnetized when cooled to T_V than the corresponding monoclinic phase remanence when warmed from 10 K. In turn, the contrasting signatures in crossing T_V are determined by the amount of remanence remaining to be demagnetized on reaching the Verwey transition region—most of the 10-K remanence but virtually none of the 300-K remanence. Unfortunately, the massive demagnetization of the monoclinic phase remanence masks any subtle details like those we see in the cubic → monoclinic transformation.

The Verwey transition temperature T_V at which the structural transformation occurs has some variability (Table 2). For annealed samples, apart from two rather uncertain determinations, T_V measured in cooling 300-K saturation remanence decreases steadily with decreasing grain size from 120 to 122 K for the 110 and 135 μm samples to 112 K for the 1 μm sample. On the face of it, this might be taken as evidence for some degree of oxidation of the finer grain sizes but there is no corresponding trend in the T_V values determined from warming curves of 10-K remanence, which are uniformly 110–114 K. On the other hand, unannealed samples have higher T_V values than the annealed samples, almost all close to 120 K.

Memory and memory ratios

Memory is the spontaneous recovery on a second crossing through T_V of some fraction of the remanence that was lost on the first crossing. In Fig. 2, the 1, 6 and 9 μm samples have small memories after warming: Their remanences above T_V and at room temperature are higher than they were below T_V. The 14 μm sample has a dip in remanence at T_V, then a modest recovery with further warming, but the remanence at 300 K is scarcely larger than it was at 100 K: the memory is negligible.

Memory of low-temperature remanence is not paleomagnetically useful but is interesting nonetheless. In Fig. 6, the unannealed magnetites without exception have no memory: The remanences at 10 K after a full warming–cooling cycle (the individual points near the left axis) are identical to the half-cycle remanences measured at 300 K. The annealed magnetites do have significant memories (Fig. 7); the fractional remanences recovered between 300 K and 10 K being smallest for the 1 μm sample and largest for the 135 μm sample. Thus, low-temperature remanence of monoclinic magnetite does preserve some memory of its original domain configurations after conversion to the cubic phase and back. To our knowledge, this behavior has not been noted before.

The mechanism of conventional memory—that of room temperature remanence of the cubic phase—has been clarified by the TEM observations of Kasama et al. (2013). Their initial Lorentz images at 143 K showed large magnetic domains separated by 90° or 180° DWs. At 103 K after zero-field cooling, the domains were smaller and were separated by 180° DWs. In spite of the change of phase and anisotropy, there was a good correspondence between magnetization directions observed (from electron holograms) above and below T_V, particularly near the specimen edge where self-demagnetizing effects come into play. In the final remanent states recorded after zero-field warming back to 143 K, large domains redeveloped. Despite some differences in positions of specific DWs, the overall pattern of domains and magnetization directions roughly matched that seen initially at 143 K.

It seems clear that the uniaxial domain structure in the monoclinic phase below T_V preserves a template sufficient to renucleate a partial replica of the initial multiaxial domain pattern on rewarming above T_V, as has long been speculated in the literature (e.g., Kobayashi and Fuller 1968). The directional stability of saturation remanence in cycling through the Verwey transition (Smirnov and Tarduno 2011) lends further support to this model. If the monoclinic phase can act as a bridge preserving overall memory of cubic phase remanence, it seems likely that the dip and recovery of remanence (or "positive anomaly") at and immediately below T_V is also a result of linkage between domain structures on either side of the transition. Detailed observations of domain structures within 10–15 K of T_V are needed to test this idea.

Conclusions

We have made a systematic study of remanence cycling as a function of grain size in magnetites ranging from small PSD (≈1 μm) to moderate MD (100–150 μm) sizes and a less thorough investigation of the effect of internal stress, through the use of matching unannealed and annealed sample sets. The magnetites all originated from natural pure crystals. Internal strain resulted from varying amounts of crushing and milling before separation into size fractions. Our results are compatible with those of previous studies of crushed natural magnetite (Hartstra 1982, 1983; Kosterov 2003) but differ significantly from observations on high internal stress glass ceramic magnetites (Halgedahl and Jarrard 1995) and low-stress

hydrothermal magnetites (Muxworthy and McClelland 2000; Özdemir et al. 2002).

A possible phase transition from monoclinic to another phase of magnetite around 50 K seems more likely to be a temperature at which the anisotropy and/or magnetostriction constants begin to increase. The evidence against a transition is that only the finest annealed grains (<9 μm) have a convincing inflection in their 10-K remanence warming curves at this temperature, that unannealed grains of all sizes have no indication of such a transition, and that cooling and warming curves of 300-K remanences for all samples also lack the transition. Coercive forces of the finer grained magnetites increase around 50 K (Dunlop et al. 2018, Figs. 5, 6), although they do not continue to increase at lower temperatures. However, IRM acquisition curves show that the entire spectrum of coercivities is multiplied almost two-fold between 50 and 10 K (Fig. 1).

One of the striking features of our cycling experiments is the very different behavior of monoclinic magnetite when it is magnetized at low temperature and warmed in zero field through T_V as opposed to being magnetized as cubic magnetite at room temperature and converted to monoclinic magnetite by zero-field cooling through T_V. Previous authors have remarked on this contrast (e.g., Muxworthy and McClelland 2000), but it is less surprising when the contrasting domain structures and anisotropies at 10 K and 300 K are taken into account. Hysteresis results (Muxworthy 1999; Özdemir et al. 2002; Dunlop et al. 2018) show that domain structure becomes more MD-like as magnetite's anisotropy and magnetostriction decrease en route to T_V, then abruptly revert to PSD-like in the much higher anisotropy monoclinic phase below T_V, ultimately approaching SD-like behavior at 10 K. In the simplest terms, DWs abound and move readily when cubic magnetite is cooled from 300 K; at T_V there is little or no remanence remaining to be demagnetized. But when monoclinic magnetite is warmed from 10 K the few DWs available are strongly pinned at twin boundaries or crystal defects; massive demagnetization can only occur with the massive drop in anisotropy and infusion of new mobile DWs near T_V. Although simplistic, we believe this is the basic reason for the contrasting cycling curves of Figs. 2, 6 and 7.

An interesting and unexplained detail of some cycling curves of room temperature remanence is a small to pronounced minimum at T_V, particularly in warming curves (Figs. 3, 4, 5). Where the minimum is well developed there is an accompanying peak in both warming and cooling curves centered on 100–105 K. In cooling, this represents a spontaneous recovery of remanence lost in crossing the Verwey transition. This dip-and-recovery phenomenon has been widely observed but not convincingly explained. It is absent from samples with significant internal stress and from natural magnetites below about 15 μm in size. But artificial magnetites produced in a low-stress hydrothermal environment exhibit dips and peaks near T_V in small grains and lack them in ≈100 μm grains (Muxworthy and McClelland 2000; Özdemir et al. 2002). The key may lie in the rather unexpected similarity between uniaxial monoclinic magnetization directions below T_V and the corresponding cubic multiaxial patterns and $\boldsymbol{M}_s$ vectors above T_V, as demonstrated by Kasama et al. (2013). What is recovered on a small scale over a few tens of degrees can evidently be retained as remanence memory over the broad temperature range of the entire cycling experiment.

Remanence memories are rather small for our samples if memory is taken to be strictly the recovery of remanence between the monoclinic and cubic phase on the second passage of T_V. A more utilitarian definition would be simply the fraction of initial remanence that survives the double passage through T_V, and is available for paleomagnetic measurement. From this viewpoint, our samples retain respectable working memories, ranging from 20 to 40% for the 1–14 μm annealed samples. It is interesting that the same samples also have measurable although smaller memories, by either definition, when given a saturation remanence at 10 K and cycled to 300 K and back (Fig. 7). Unfortunately, the various memory ratios are too scattered as a function of grain size to have potential as granulometric indicators (Fig. 9).

Authors' contributions

DD as the senior author gathered the majority of the data and did most of the writing of the manuscript. ÖÖ participated in the data gathering and ongoing discussions of the meaning and interpretation of results. Both authors read and approved the final manuscript.

Acknowledgements

Research supported by the Natural Sciences and Engineering Research Council of Canada. Thanks to Mike Jackson, Bruce Moskowitz and Peat Sølheid for their discussions and help during our visits to the Institute for Rock Magnetism, which is operated with support from the National Science Foundation, Earth Sciences Division and the University of Minnesota. Measurements at Kyoto University were taken during a visit funded by the Japan Society for the Promotion of Science. We thank Prof. Masayuki Torii for hosting our visit and participating actively in the measurements. Constructive reviews by Aleksey Smirnov, Andrei Kosterov and Adrian Muxworthy improved the paper. As stated in the Acknowledgments, Mike Jackson, Bruce Moskowitz and Peat Sølheid of the staff of the Institute for Rock Magnetism, University of Minnesota, helped in setting up experiments and informal discussions of the data but did not participate actively in the data gathering and final interpretation. Prof. Masayuki Torii took a more active role in the measurements at Kyoto University because of his greater experience with the instruments used. He has, however, specifically declined to be included as an author on the paper. All these colleagues are agreeable to being acknowledged.

Competing interests

The authors declare that they have no competing interests.

Availability of data and materials
The datasets used and/or analyzed during the current study are available from the corresponding author on reasonable request.

Funding
The sources of funding for the research reported were the Natural Sciences and Engineering Research Council of Canada (Grant No. A7709) and the Japan Society for the Promotion of Science, as declared in the Acknowledgments. Neither funding body had any direct influence on the design of the study or the collection, analysis and interpretation of data or on the writing of the manuscript.

Publisher's Note

Received: 11 July 2018 Accepted: 18 September 2018
Published online: 04 October 2018

References

Abe K, Miyamoto Y, Chikazumi S (1976) Magnetocrystalline anisotropy of low-temperature phase of magnetite. J Phys Soc Jpn 41:1894–1902
Bickford LR, Brownlow JM, Penoyer RF (1957) Magnetocrystalline anisotropy in cobalt-substituted magnetite single crystals. Proc IEE B104:238–244
Bryson JFJ, Kasama T, Dunin-Borkowski RE, Harrison RJ (2013) Ferrimagnetic/ferroelastic domain interactions in magnetite below the Verwey transition: II. Micromagnetic and image simulations. Phase Transit 86:88–102. https://doi.org/10.1080/01411594.2012.695372
Carter-Stiglitz B, Moskowitz B, Solheid P, Berquo TS, Jackson M, Kosterov A (2006) Low-temperature behavior of multidomain titanomagnetites: TM0, TM16, and TM35. J Geophys Res 111:B12S05. https://doi.org/10.1029/2006jb004561
Chikazumi S, Chiba K, Suzuki T, Yamada T (1971) Electron microscopic observation of low temperature phase of magnetite. In: Hoshino Y, Iida S, Sugimoto M (eds) Ferrites: proceedings of international conference. University of Tokyo Press, pp 141–143
Creer KM, Like CB (1967) A low temperature investigation of the natural remanent magnetization of several igneous rocks. Geophys J R Astr Soc 12:301–312
Dunlop DJ (2002) Theory and application of the Day plot (M_{rs}/M_s/vs. H_{cr}/H_c), 1. Theoretical curves and tests using titanomagnetite data. J Geophys Res 107(B3):2056. https://doi.org/10.1029/2001JB000486
Dunlop DJ (2003) Stepwise and continuous low-temperature demagnetization. Geophys Res Lett 30:1582. https://doi.org/10.1029/2003GL017268
Dunlop DJ (2014) High-temperature susceptibility of magnetite: a new pseudo-single-domain effect. Geophys J Int 199:707–716. https://doi.org/10.1093/gji/ggu247
Dunlop DJ, Özdemir Ö, Xu S (2018) Magnetic hysteresis of 0–6-110 μm magnetites across the Verwey transition. Can J Earth Sci. https://doi.org/10.1139/cjes-2018-0088
Halgedahl SL, Jarrard RD (1995) Low-temperature behavior of single-domain through multidomain magnetite. Earth Planet Sci Lett 130:127–139
Harrison RJ, Dunin-Borkowski RE, Putnis A (2002) Direct imaging of nanoscale magnetic interactions in minerals. Proc Natl Acad Sci USA 99:16556–16561
Hartstra RL (1982) A comparative study of the ARM and I_{sr} of some natural magnetites of MD and PSD grain size. Geophys J R Astr Soc 71:497–518
Hartstra RL (1983) TRM, ARM and Isr of two natural magnetites of MD and PSD grain size. Geophys J R Astr Soc 73:719–737
Heider F, Dunlop DJ, Soffel HC (1992) Low-temperature and alternating field demagnetization of saturation remanence and thermoremanence in magnetite grains (0.037 μm to 5 mm). J Geophys Res 97:9371–9381
Hodych JP (1986) Evidence for magnetostrictive control of intrinsic susceptibility and coercive force of multidomain magnetite in rocks. Phys Earth Planet Inter 42:184–194
Hodych JP (1991) Low-temperature demagnetization of saturation remanence in rocks bearing multidomain magnetite. Phys Earth Planet Inter 66:144–152
Kakol Z, Sabol J, Honig JM (1991) Magnetic anisotropy of titanomagnetites $Fe_{3-x}Ti_xO_4$, $0<x<0.55$. Phys Rev B44:2198–2204
Kakol Z, Sabol J, Stickler J, Kozlowski A, Honig JM (1994) Influence of titanium doping on the magnetocrystalline anisotropy of magnetite. Phys Rev B49:12767–12772
Kasama T, Church NS, Feinberg JM, Dunin-Borkowski RE, Harrison RJ (2010) Direct observation of ferrimagnetic/ferroelastic domain interactions in magnetite below the Verwey transition. Earth Planet Sci Lett 297:10–17. https://doi.org/10.1016/j.epsl.2010.05.004
Kasama T, Harrison RJ, Church NS, Nagao M, Feinberg JM, Dunin-Borkowski RE (2013) Ferrimagnetic/ferroelastic domain interactions in magnetite below the Verwey transition: I. Electron holography and Lorentz microscopy. Phase Transit 86:67–87. https://doi.org/10.1080/01411594.2012.695373
King JG, Williams W (2000) Low-temperature magnetic properties of magnetite. J Geophys Res 105:16427–16436
Kobayashi K, Fuller M (1968) Stable remanence and memory in multidomain materials with special reference to magnetite. Philos Mag 18:601–624
Kosterov A (2001) Magnetic hysteresis of pseudo-single-domain and multidomain magnetite below the Verwey transition. Earth Planet Sci Lett 186:245–253
Kosterov A (2003) Low-temperature magnetization and AC susceptibility of magnetite: effect of thermomagnetic history. Geophys J Int 154:58–71
Kosterov A, Fabian K (2008) Twinning control of magnetic properties of multidomain magnetite below the Verwey transition revealed by measurements on individual particles. Geophys J Int 174:93–106. https://doi.org/10.1046/j.1365-246X.2008.03811.x
Medrano C, Schlenker M, Baruchel J, Espeso J, Miyamoto Y (1999) Domains in the low-temperature phase of magnetite from synchrotron-radiation X-ray topographs. Phys Rev B59:1185–1195
Merrill RT (1970) Low-temperature treatment of magnetite and magnetite-bearing rocks. J Geophys Res 75:3343–3349
Moloni K, Moskowitz BM, Dahlberg ED (1996) Domain structures in single crystal magnetite below the Verwey transition as observed with a low-temperature magnetic force microscope. Geophys Res Lett 23:2851–2854
Muxworthy AR (1999) Low-temperature susceptibility and hysteresis of magnetite. Earth Planet Sci Lett 169:51–58
Muxworthy AR, McClelland E (2000) The causes of low-temperature demagnetization of remanence in multidomain magnetite. Geophys J Int 140:115–131
Muxworthy AR, Williams W (2006) Low-temperature viscous magnetization of multidomain magnetite: evidence for disaccommodation contribution. J Magn Magn Mater 307:113–119
Muxworthy AR, Dunlop DJ, Özdemir Ö (2003) Low-temperature cycling of isothermal and anhysteretic remanence: microcoercivity and magnetic memory. Earth Planet Sci Lett 205:173–184
Otsuka N, Sato H (1986) Observation of the Verwey transition in Fe_3O_4 by high-resolution electron microscopy. J Solid State Chem 61:212–222
Özdemir Ö (2000) Coercive force of single crystals of magnetite at low temperatures. Geophys J Int 141:351–356
Özdemir Ö, Dunlop DJ (1998) Single-domain-like behavior in a 3-mm natural single crystal of magnetite. J Geophys Res 103:2549–2562
Özdemir Ö, Dunlop DJ (1999) Low-temperature properties of a single crystal of magnetite oriented along principal magnetic axes. Earth Planet Sci Lett 165:229–239
Özdemir Ö, Xu S, Dunlop DJ (1995) Closure domains in magnetite. J Geophys Res 100:2193–2209
Özdemir Ö, Dunlop DJ, Moskowitz BM (2002) Changes in remanence, coercivity and domain state at low temperature in magnetite. Earth Planet Sci Lett 194:343–358
Özdemir Ö, Dunlop DJ, Jackson M (2009) Frequency and field dependent susceptibility of magnetite at low temperature. Earth Planets Space 61:125–131. https://doi.org/10.1186/BF03352892
Ozima M, Ozima M, Nagata T (1964) Low temperature treatment as an effective means of 'magnetic cleaning' of natural remanent magnetization. J Geomagn Geoelectr 16:37–40
Roberts AP, Almeida TP, Church NS, Harrison RJ, Heslop D, Li Y, Li J, Muxworthy AR, Williams W, Zhao X (2017) Resolving the origin of pseudo-single

domain magnetic behavior. J Geophys Res Solid Earth 122:9534–9558. https://doi.org/10.1002/2017JB014860
Salje EKH (1993) Phase transitions in ferroelastic and co-elastic crystals. Cambridge University Press, Cambridge, p 365
Smirnov AV (2006) Memory of the magnetic field applied during cooling in the low-temperature phase of magnetite: grain-size dependence. J Geophys Res 111:B12S04. https://doi.org/10.1029/2006JB004573
Smirnov AV (2009) Grain-size dependence of low-temperature remanent magnetization in natural and synthetic magnetite: experimental study. Earth Planets Space 61:119–124. https://doi.org/10.1186/BF03352891
Smirnov AV, Tarduno JA (2002) Magnetic field control of the low-temperature magnetic properties of stoichiometric and cation-deficient magnetite. Earth Planet Sci Lett 194:359–368
Smirnov AV, Tarduno JA (2011) Development of a low-temperature insert for the measurement of remanent magnetization direction using superconducting quantum interference device rock magnetometers. Geochem Geophys Geosyst 12(4):Q04Z23. https://doi.org/10.1029/2011GC003517
Syono Y (1965) Magnetocrystalline anisotropy and magnetostriction of Fe_3O_4–Fe_2TiO_4 series with special application to rock magnetism. Jpn J Geophys 4:71–143
Tsuya N, Arai KI, Ohmori K (1977) Effect of magnetoelastic coupling on the anisotropy of magnetite below the transition temperature. Physica 86–88B:959–960
Verwey EJW (1939) Electronic conduction of magnetite (Fe_3O_4) and its transition point at low temperatures. Nature 44:327–328
Walz F (2002) The Verwey transition—a topical review. J Phys Cond Matter 14:R285–R340
Walz F, Kronmüller H (1991) Evidence for a single-stage Verwey transition in perfect magnetite. Philos Mag B64:623–628
Worm H-U, Markert H (1987) Magnetic hysteresis properties of fine-particle titanomagnetites precipitated in a silicate matrix. Phys Earth Planet Inter 46:84–92
Xu S, Merrill RT (1989) Microstress and microcoercivity in multi-domain grains. J Geophys Res 94:10627–10636
Yu Y, Tauxe L, Moskowitz BM (2004) Temperature dependence of magnetic hysteresis. Geochem Geophys Geosyst 5:Q06H11. https://doi.org/10.1029/2003GC000685